Vector detection of ac magnetic fields by nitrogen vacancy centers of single orientation in diamond

Pooja Lamba [1,*] Akshat Rana [1,*] Sougata Halder [2] Siddharth Dhomkar [3,4] Dieter Suter [5]
and Rama K. Kamineni [1,6,†]

[1]*Department of Physics, Bennett University, Greater Noida 201310, India*
[2]*Department of Physics, IIT Jodhpur, Jodhpur 342030, India*
[3]*Department of Physics, IIT Madras, Chennai 600036, India*
[4]*Center For Quantum Information, Communication And Computing, IIT Madras, Chennai 600036, India*
[5]*Fakultät Physik, Technische Universität Dortmund, D-44221 Dortmund, Germany*
[6]*SIAS, Krea University, Sri City 517646, India*

Nitrogen vacancy (NV) centers in diamond have useful properties for detecting both ac and dc magnetic fields with high sensitivity at nanoscale resolution. The vector detection of ac magnetic fields can be achieved by using NV centers having three different orientations. Here, we propose a method to achieve this by using NV centers of single orientation. In this method, a static magnetic field is applied perpendicular to the NV axis, leading to strong mixing of the $m_s = -1$ and 1 electron spin states. As a result, all three electron spin transitions of the triplet ground state have nonzero dipole moments, with each transition coupling to a single component of the magnetic field. This can be used to measure both the strength and orientation of the applied ac field. To validate the technique, we perform a proof-of-principle experiment using a subset of ensemble NV centers in diamond, all having the same orientation. This method is equally applicable to single NV centers.

I. INTRODUCTION

Sensitive detection of magnetic fields is an essential task in many areas of science, technology, and medicine. Sensors based on different techniques have been developed for this purpose [1–4]. Among these, sensors based on nitrogen vacancy (NV) centers in diamond have the advantages of room-temperature operation and high-sensitivity detection with nanoscale resolution [5–7]. Additionally, NV centers are useful for detecting both ac and dc magnetic fields [8–15].

Sensitive detection of ac magnetic fields produced by spins and charges at micro- and nanoscales have interesting applications in magnetic resonance and condensed matter physics. Methods based on different technologies have been developed for this purpose [16–23]. In many cases, it is desirable to measure not only the magnitude, but also the orientation of the magnetic fields. Important examples where the vector detection of ac fields is important include magnetic excitations and current distributions in materials [24]. Most of the existing methods for detecting ac magnetic fields in the microwave (MW) frequency range lack vector detection capabilities or nanoscale resolution.

Small sensor size, long-coherence times, and C_{3v} symmetry of NV centers can be beneficial for the vector detection of dc and ac magnetic fields. The vector detection of dc and slow time-varying fields by using NV centers have been thoroughly investigated [25–33]. Here, we focus on the vector detection of fields with frequency greater than 1 MHz. For small static magnetic fields, the quantization axis of NV centers is pointed along the NV axis. The electron spin dipole moments, in general, are perpendicular to the quantization axis and hence only the components of the applied ac fields that are perpendicular to the quantization axis interact with the spin transitions of the center. Therefore, to achieve the vector detection of ac fields using conventional technique, at least, three NV centers having varied orientations are essential. This has been demonstrated by using ensemble NV centers [34]. However, the requirement of multiple NV centers with different orientations puts a restriction on the sensor size and limits its applicability for nanoscale imaging. Recently, vector detection of ac magnetic fields by a single NV center has been demonstrated by using a method known as rotating-frame Rabi magnetometry [35]. In Ref. [35], the components of the applied ac field have been measured by tuning the Rabi frequencies of NV spin transitions to different resonance conditions. However, this method requires that the Rabi frequencies of the electron spin transitions are comparable to their transition frequencies, which is a stringent prerequisite. A vector detection scheme using level anticrossings of an NV center coupled to a first-shell ^{13}C nuclear spin has been reported in Ref. [36]. The anticrossings used in Ref. [36] occur when the energy level splitting due to the Zeeman interaction of the NV electron spin is equal to the splitting due to the hyperfine interaction of first-shell ^{13}C nuclear spin. The disadvantage of this method is that it requires a first-shell ^{13}C atom; the probability of finding such a configuration is merely 3.3%. Moreover, the bandwidth of the sensor is very narrow.

NV centers with a transverse magnetic field have been previously used for electric-field sensing [37], suppression of

---

*These authors contributed equally to this work.
†koti.kamineni@gmail.com

electron spin decoherence [36,38], temperature sensing [39], and magnetic field angle sensing [40].

Here, we propose and demonstrate a method for the vector detection of ac magnetic fields via NV centers of single orientation. This method, which is also applicable for single NV centers, exploits the energy level anticrossing that occurs within the $m_S = \pm1$ subspace when a static magnetic field is applied perpendicular to the NV axis. Particularly, for magnetic fields of strength up to few tens of mT, the eigenstates of the electron spin of the center at this level anticrossing can be approximately written as $|0\rangle$, $\frac{|-1\rangle-|1\rangle}{\sqrt{2}}$, and $\frac{|-1\rangle+|1\rangle}{\sqrt{2}}$, where $|m_S\rangle = |0\rangle, |\pm1\rangle$ refer to the eigenstates of the electron spin operator S_z and z is orientated along the symmetry axis of the NV center. All three transitions between these levels, including the transition in the $m_S = \pm1$ subspace, have strong dipole moments and their directions are perpendicular to each other. Only the component of the applied ac field that is oriented parallel to the dipole moment can excite the corresponding transition. This can be used to measure both strength and orientation of the applied ac field. The amplitude of the vector components of the ac field can be measured by on-resonantly exciting each of the three transitions. The frequencies of these transitions can be tuned to match the frequency of the ac field by varying the strength of the static magnetic field.

This paper is arranged as follows. In Sec. II, we describe the method, and in Sec. III, we demonstrate the method experimentally by using an ensemble of identically oriented NV centers in diamond. Finally, in Sec. IV, we discuss and conclude.

II. METHODOLOGY

The NV center is a point defect in diamond with C_{3v} symmetry [41,42]. It has spin-1 ground and excited states. Optical pumping causes polarization of its electron spin into the $m_S = 0$ state. Since the intensity of the fluorescence emitted by the center depends on its spin state, it is possible to read the spin state of the center optically. The Hamiltonian for the electron spin of the ground state of the NV center in an applied static magnetic field can be written as

$$\mathcal{H}_0 = DS_z^2 + \gamma_e B(\sin\theta\, S_x + \cos\theta\, S_z). \quad (1)$$

Here, we set $h = 1$ and use frequency units for energy. $S_{x/y/z}$ represent the components of the spin-1 angular momentum operator. $D = 2870$ MHz is the zero-field splitting between the $|m_S\rangle = |0\rangle$ and $|\pm1\rangle$ states. γ_e represent the gyromagnetic ratio of the electron spin. B and θ represent the strength and polar angle of the static magnetic field in a coordinate system whose Z axis is aligned with the symmetry axis of the center, as shown in Fig. 1(a). For $\theta \neq 0$, the X axis is defined as the direction of the projection of the field into the plane perpendicular to the Z axis.

The $|m_S\rangle = |\pm1\rangle$ states, which are degenerate in zero magnetic field, split due to the Zeeman interaction and this splitting is proportional to the strength of the applied static magnetic field. When the field is applied parallel to the NV axis or at a small angle to it, m_S is a good quantum number and the eigenstates of the electron spin are $|0\rangle$, $|-1\rangle$, and $|1\rangle$. As shown in Fig. 1(b), the transitions $|0\rangle \longleftrightarrow |-1\rangle$ and $|0\rangle \longleftrightarrow |1\rangle$ are allowed and the transition between the states
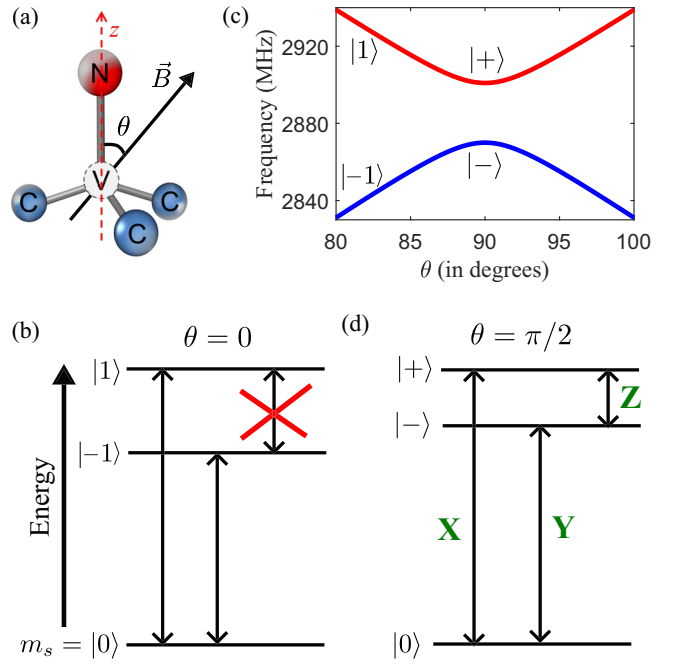

FIG. 1. (a) Schematic diagram of the NV center in diamond and the static magnetic field. (b) Energy level diagram of the ground state of the NV center and the allowed transitions between them when $\vec{B}$ is oriented parallel to the NV axis. (c) Frequencies of energy levels of the $m_S = \pm1$ subspace as a function of θ for $B = 10.7$ mT. (d) Energy level diagram when $\vec{B}$ is oriented perpendicular to the NV axis. The transition labeled by Z has a dipole moment along the NV axis, the transition labeled by X has a dipole moment along the direction of $\vec{B}$, and the transition labeled by Y has a dipole moment perpendicular to both these directions.

$|-1\rangle$ and $|1\rangle$ is forbidden. The transition dipole moments of the allowed transitions are oriented perpendicular to the NV axis and thus can be excited by components of resonant microwave fields that are oriented perpendicular to the NV axis.

When the angle between the NV axis and the static magnetic field is close to $\pi/2$, there is a strong mixing between the states $|m_S\rangle = |-1\rangle$ and $|1\rangle$. As shown in Fig. 1(c), the plot of energy levels versus angle θ shows anticrossing at $\theta = \pi/2$. For magnetic fields of strength up to few tens of mT, the eigenstates of the electron spin at $\theta = \pi/2$ can be approximately written as $|0\rangle$, $|-\rangle$, and $|+\rangle$, where $|-\rangle$ and $|+\rangle$ are defined as $\frac{1}{\sqrt{2}}(|-1\rangle - |1\rangle)$ and $\frac{1}{\sqrt{2}}(|-1\rangle + |1\rangle)$, respectively. The separation between the states $|-\rangle$ and $|+\rangle$ is of the order of $\frac{(\gamma_e B)^2}{D}$. All three transitions between the states $|0\rangle$, $|-\rangle$, and $|+\rangle$ are allowed and have strong dipole moments [Fig. 1(d)]. Most importantly, the orientations of dipole moments of these transitions are orthogonal to each other. The dipole moment of the transition between the states $|-\rangle$ and $|+\rangle$ is parallel to the NV axis, the dipole moment of the transition between the states $|0\rangle$ and $|+\rangle$ is along the direction of the magnetic field, and the dipole moment of the transition between the states $|0\rangle$ and $|-\rangle$ is oriented perpendicular to both these directions. In the coordinate system defined earlier in this section, $|\langle -|S_z|+\rangle| \approx 1$, $|\langle 0|S_x|+\rangle| \approx 1$, and $|\langle 0|S_y|-\rangle| \approx 1$, while all other matrix elements are close to zero. This can be
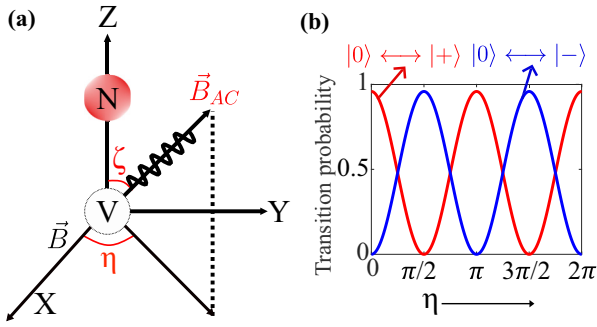
(a)

(b)

FIG. 2. (a) Coordinate system with static and ac magnetic field orientations. (b) Transition probabilities of $|0\rangle \longleftrightarrow |+\rangle$ and $|0\rangle \longleftrightarrow |-\rangle$ transitions as a function of η for $\theta = \pi/2$.

utilized for the vector detection of ac magnetic fields that are on resonance with these transitions.

A linearly polarized ac magnetic field can be expressed as

$$\vec{B}_{ac} = B_{ac}(\sin\zeta\cos\eta\,\hat{x} + \sin\zeta\sin\eta\,\hat{y} + \cos\zeta\,\hat{z}) \\ \times \cos(\omega t + \varphi), \quad (2)$$

where B_{ac}, ζ, and η are the strength, polar, and azimuthal angles of the field, respectively. ω and φ are the angular frequency and phase of the field. A schematic representation of $\vec{B}_{ac}$, and the angles ζ and η is given in Fig. 2(a). The Hamiltonian corresponding to the interaction of the ac field with the electron spin of the NV center can be written as

$$\mathcal{H}_{ac} = \gamma_e \vec{B}_{ac} \cdot \vec{S}. \quad (3)$$

The purpose of this paper is to determine the parameters B_{ac}, ζ, and η of the ac field from experimental measurements. As shown in Fig. 2(b), the probabilities of the transitions $|0\rangle \longleftrightarrow |-\rangle$ and $|0\rangle \longleftrightarrow |+\rangle$ have a sinusoidal dependence on the angle η between the static field and the transverse component of the ac field. When $\eta = 0$ ($\eta = \pi/2$), the probability of the transition $|0\rangle \longleftrightarrow |-\rangle$ ($|0\rangle \longleftrightarrow |+\rangle$) is close to zero and the probability of $|0\rangle \longleftrightarrow |+\rangle$ ($|0\rangle \longleftrightarrow |-\rangle$) is close to one. Therefore, by comparing the experimental amplitudes or Rabi frequencies of the aforementioned transitions for a fixed transverse orientation of the static field, we can determine the angle η. Once η is known, B_{ac} and ζ can be determined by comparing the Rabi frequencies of the transition $|-\rangle \longleftrightarrow |+\rangle$ and any one of the two transitions $|0\rangle \longleftrightarrow |-\rangle$ and $|0\rangle \longleftrightarrow |+\rangle$. When the frequency of the applied ac field matches the frequency of the transitions, whose dipole moment is along the direction of the field, it induces transitions, which may be observed as a drop in the fluorescence emitted by the NV centers under optical illumination. This effect is known as optical detection of magnetic resonance (ODMR) [43,44]. The relative amplitudes of the resonant dips of the three transitions in the continuous-wave (cw) ODMR experiments can be used to determine the parameters of the ac field. Alternatively pulsed ODMR experiments as described in the next section can be performed to measure the Rabi frequencies of the transitions.

For a fixed static field, the transition frequency of the transition $|-\rangle \longleftrightarrow |+\rangle$ is very different from that of the transitions $|0\rangle \longleftrightarrow |-\rangle$ and $|0\rangle \longleftrightarrow |+\rangle$. So, vector

detection at a fixed static field requires tuning of the frequency of the ac field to frequencies of the transitions $|0\rangle \longleftrightarrow |-\rangle$ and $|-\rangle \longleftrightarrow |+\rangle$. Vector detection of an ac field of fixed frequency requires application of two different static magnetic field strengths. In the next section, we describe the experimental implementation of the protocol at a fixed static field of strength 10.7 mT. We discuss the procedure for the vector detection of an ac field of fixed frequency in the last section.

III. PROOF-OF-PRINCIPLE EXPERIMENTS

The experiments were performed on a home-built confocal microscope setup equipped with a 532-nm laser for off-resonant excitation of optical transitions, and radio-frequency (rf) and MW electronic circuits for resonant excitation of electron spin transitions. A chemical vapor deposition (CVD)-grown single-crystal diamond with a nitrogen concentration of 800 ppb was used. There were hundreds of NV centers within the excitation volume of the confocal microscope. The ac magnetic fields, whose vector detection we were trying to achieve, was generated by a current through a 25-μm copper wire attached to the diamond surface. This work required precise orientation of the static magnetic field with respect to the NV axis and it was achieved by using a permanent magnet attached to two rotational stages whose axes were orthogonal to each other and crossed at the site of the diamond crystal. NV centers of all four possible orientations that were within the confocal spot were excited simultaneously by the laser and contributed to the total detected fluorescence. However, in the ODMR experiments, the frequency of the applied field selects only one specific orientation.

As described in the previous section, we determine η, the angle between the transverse component of the ac field and the static magnetic field. Specifically, Fig. 1(d) illustrates that when the static magnetic field is oriented perpendicular to the NV axis, the transition between the states $|0\rangle$ and $|+\rangle$ can only be excited by a component of the ac field that is parallel to the static magnetic field. Likewise, the transition between the states $|0\rangle$ and $|-\rangle$ can be excited by a component of the ac field that is perpendicular to both static field and NV axis. In our experimental setup, the direction of the applied ac field is fixed, but we can change the direction of the static magnetic field. We recorded cw ODMR spectra by applying a static magnetic field of strength 10.7 mT at different orientations in the plane perpendicular to the NV axis. Figure 3 summarizes the results. When $\eta = 0$, the ODMR consists of only one peak at 2932 MHz corresponding to the $|0\rangle \longleftrightarrow |+\rangle$ transition. The other peak at 2900 MHz corresponding to the transition $|0\rangle \longleftrightarrow |-\rangle$ has negligible intensity. Conversely, when $\eta = \pi/2$, the peak at 2932 MHz is of negligible intensity compared to the peak at 2900 MHz. When $\eta = \pi/4$, as shown in Fig. 3(c), both peaks are of equal intensity. In other words, when the static magnetic field is aligned with the transverse component of the ac field, the transition $|0\rangle \longleftrightarrow |-\rangle$ has minimum intensity and the transition $|0\rangle \longleftrightarrow |+\rangle$ has maximum intensity. So, we can determine the direction of the transverse component of the ac field by simply rotating the static magnetic field in the plane perpendicular to the NV axis and look for the direction at which the transition $|0\rangle \longleftrightarrow |-\rangle$ has minimum intensity and the transition $|0\rangle \longleftrightarrow |+\rangle$ has
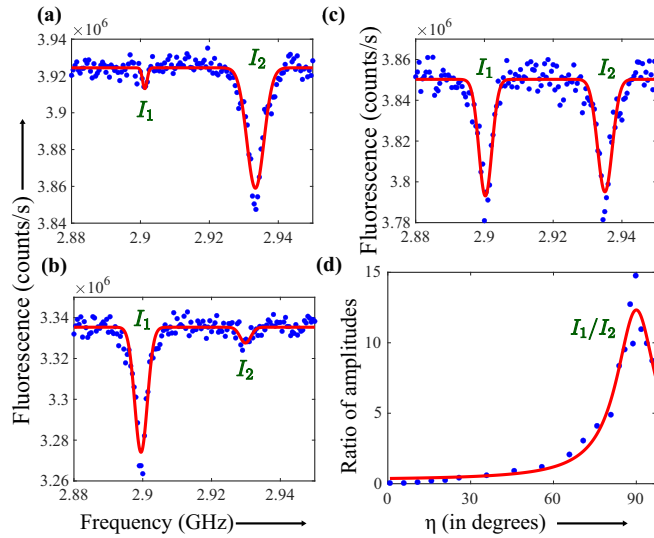
FIG. 3. cw ODMR spectra for different orientations of the static magnetic field in the plane perpendicular to the NV axis: (a) $\eta = 0$, (b) $\eta = \pi/2$, (c) $\eta = \pi/4$. Blue dots represent experimental data and red lines are Gaussian fits of these data. (d) Ratio of amplitudes, I_1/I_2, as a function of η. Blue dots represent the ratio of amplitudes determined from the ODMR spectra and the red line represents a fit of these data to the expression $a\frac{b}{(\eta-\eta_0)^2+b^2} + c$, where $\eta_0 = 90°$ (± 0.9).

maximum intensity. The ratio of intensities of these two transitions as a function of η is given in Fig. 3(d). The maximum of this ratio corresponds to $\eta = \pi/2$. From this, we are able to determine the direction of the transverse component of the ac field with an uncertainty $\pm 0.9°$. Alternatively, one can also determine this at a given magnetic field orientation in the transverse plane by comparing the Rabi frequencies of the two transitions.

As mentioned in the last section, B_{ac}, the strength of the applied ac field, and ζ, the angle between the NV axis and the direction of the ac field, can be determined from the measured Rabi frequencies of the transitions $|0\rangle \longleftrightarrow |-\rangle$ and $|-\rangle \longleftrightarrow |+\rangle$ for a fixed value of η. The Rabi oscillations of the transition $|0\rangle \longleftrightarrow |-\rangle$ can be straightforwardly measured by using the pulse sequence given in Fig. 4(b) and the result is shown in Fig. 4(d).

The transition frequency of the transition $|-\rangle \longleftrightarrow |+\rangle$ is equal to the difference between those of the transitions $|0\rangle \longleftrightarrow |-\rangle$ and $|0\rangle \longleftrightarrow |+\rangle$. From the ODMR spectra in Fig. 3, it is determined as 32 MHz. Laser illumination does not create a population difference between the states $|-\rangle$ and $|+\rangle$ and also these states cannot be distinguished directly from the intensity of the fluorescence emitted by the NV centers. So, to measure the Rabi oscillations of the transition $|-\rangle \longleftrightarrow |+\rangle$, the pulse sequence given in Fig. 4(c) is used. First, the state $|0\rangle$ is populated by a laser pulse and this population is transferred to the $|-\rangle$ state by a microwave π pulse. This creates population difference between the states $|-\rangle$ and $|+\rangle$. For the actual Rabi experiment, the transition $|-\rangle \longleftrightarrow |+\rangle$ is driven on resonance by an rf pulse with a frequency of 32 MHz and variable duration. The resulting dynamics are measured by transferring the population from $|-\rangle$ to $|0\rangle$ by the second
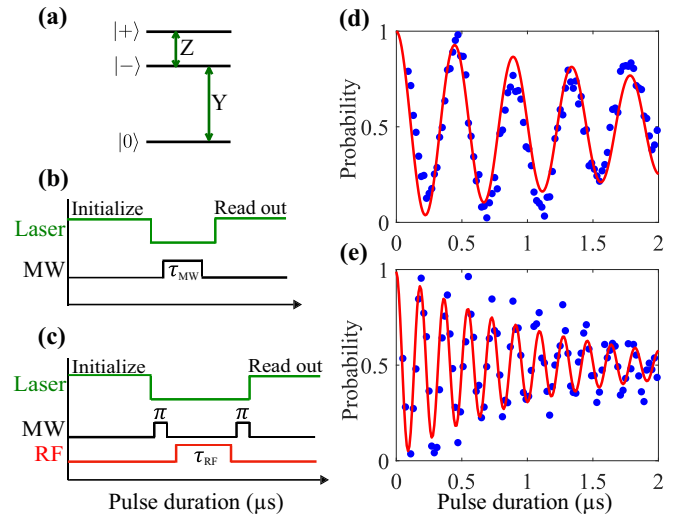

FIG. 4. Rabi oscillations and the pulse sequences. (a) Electron spin energy level diagram displaying the transitions whose Rabi oscillations are measured. (b) and (c) represent the pulse sequences, and (d) and (e) are the resultant Rabi oscillations of the transitions $|0\rangle \longleftrightarrow |-\rangle$ and $|-\rangle \longleftrightarrow |+\rangle$ respectively. MW and RF in (b) and (c) refer to the frequencies of the transitions $|0\rangle \longleftrightarrow |-\rangle$ and $|-\rangle \longleftrightarrow |+\rangle$, which are 2900 and 32 MHz, respectively. In (d) and (e), blue dots represent experimental data and red lines represent fits of this data to the expression $a\cos(2\pi\nu t)\exp(-t/T_R) + c$. $\nu = 2.24$ (± 0.01) and 5.49 (± 0.02) MHz, and $T_R = 2.9$ (± 1.4) and 1.2 (± 0.3) µs for (d) and (e), respectively.

microwave π pulse and reading it out by applying the second laser pulse. The corresponding Rabi oscillations are shown in Fig. 4(e).

The expressions relating the Rabi frequencies and the corresponding transition amplitudes can be written as

$$\sqrt{2}\frac{\gamma_e}{2\pi}B_{\text{MW}}\sin\zeta\cos\eta|\langle 0|S_x|+\rangle| = R_{0+}, \quad (4)$$

$$\sqrt{2}\frac{\gamma_e}{2\pi}B_{\text{MW}}\sin\zeta\sin\eta|\langle 0|S_y|-\rangle| = R_{0-}, \quad (5)$$

$$\sqrt{2}\frac{\gamma_e}{2\pi}B_{\text{rf}}\cos\zeta|\langle -|S_z|+\rangle| = R_{-+}. \quad (6)$$

Here, B_{MW} and B_{rf} represent the amplitudes of the ac field at frequencies 2900 and 32 MHz, respectively. $R_{0+} = 3.43$ (± 0.01) MHz, $R_{0-} = 2.24$ (± 0.01) MHz, and $R_{-+} = 5.49$ (± 0.02) MHz are the measured Rabi frequencies of the transitions $|0\rangle \longleftrightarrow |+\rangle$, $|0\rangle \longleftrightarrow |-\rangle$, and $|-\rangle \longleftrightarrow |+\rangle$, respectively. From Eqs. (4) and (5), we can write

$$\tan\eta = \frac{R_{0-}|\langle 0|S_x|+\rangle|}{R_{0+}|\langle 0|S_y|-\rangle|}, \quad (7)$$

and the angle η is 33.3° (± 0.1). As expected, this angle matches with the angle between the current magnetic field vector and the X axis, determined from the ODMR spectra earlier in this section as 34°. This validates the method for determining η.

Determining the angle ζ, and B_{MW}, B_{rf} requires accurate measurement of the ratio $\frac{B_{\text{rf}}}{B_{\text{MW}}}$ at the site of the sensor. Because of the large frequency difference between the B_{MW} and B_{rf} signals and the simple wire antenna that is used for

transmission, it is not possible to accurately determine the ratio $\frac{B_{\rm rf}}{B_{\rm MW}}$ at the site of the sensor in our experimental setup. By measuring the power levels of the MW and rf signals in the transmission line immediately after the wire antenna, we obtain an estimate of the ratio $\frac{B_{\rm rf}}{B_{\rm MW}} \approx 0.44$. By substituting this ratio and the measured Rabi frequencies into Eqs. (4) and (6), we determine $B_{\rm MW} = 0.334$ mT, $B_{\rm rf} = 0.146$ mT, and $\zeta = 18°$. To compare the direction of the measured ac field vector with the calculated one, we define a laboratory coordinate system in which the Y axis is parallel to the wire antenna and the Z axis is perpendicular to the diamond surface. In this coordinate system, the direction of the measured ac field vector is $[0.48, 0.30, -0.83]^T$. From the center of the wire antenna, the sensor is at a horizontal distance of 44 μm and the vertical distance is approximately 22 μm. Using these experimental inputs, we calculate the direction of the ac field to be $[0.45, 0, -0.89]^T$. The angle between the experimentally determined and the calculated ac field vectors is $18°$. This apparent discrepancy is a result of the uncertainty in the measurement of the ratio $\frac{B_{\rm rf}}{B_{\rm MW}}$ in the current setup. This error can be reduced by minimizing the frequency difference between the NV transitions used for the vector detection. This, in turn, can be achieved by performing the experiments at two different static magnetic field strengths instead of at one field strength. The associated procedure is described in the next section.

The sensitivity of the magnetic field measurement can be calculated by using the formula [45–47]

$$\eta_B = \delta B \sqrt{nT}, \qquad (8)$$

where δB is the uncertainty in the measurement of the ac magnetic field, n is the total number of experiments, and T is the sensing time in each experiment. From the fit of the Rabi oscillations, we estimate $\eta_B \approx 1$ μT/$\sqrt{\rm Hz}$, which is similar to the previously reported sensitivity values [34,35]. The sensitivity of the current method is mainly limited by the decay time of the Rabi oscillations. The contrast in the presented ODMR experiments is about 3%. For single NV centers, a contrast of about 30% can be expected. However, for single NV centers, the photon shot noise is higher due to the low fluorescence intensity compared to the ensembles. The photon count rate in the current experiments is roughly 100 times the count rate of single NV centers. Considering that the signal-to-noise ratio is proportional to the square root of the number of detected photons, we expect a sensitivity of the order of 1 μT/$\sqrt{\rm Hz}$ for single NV centers as well.

IV. DISCUSSION AND CONCLUSION

The experimental demonstration of the method presented in the last section uses an ac field of two different frequencies for the vector detection. However, when the vector detection of an arbitrary ac field is performed, it may not always be possible to tune its frequency. The proposed method can be used for the vector detection of an ac field of single frequency, but it requires application of a static magnetic field of two different strengths; one of them is greater than 100 mT, which is beyond the field strength that our current experimental setup can produce at the site of diamond crystal. Nevertheless, we now discuss the procedure to perform vector detection at a
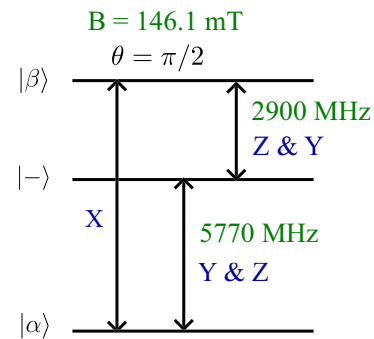

FIG. 5. Energy level diagram of the electron spin in the NV center for $B = 146.1$ mT and $\theta = \pi/2$. Here, $|\alpha\rangle = 0.82|0\rangle - 0.58|+\rangle$ and $|\beta\rangle = 0.82|+\rangle + 0.58|0\rangle$. The labels X, Y, and Z represent the orientation of the dipole moment of the corresponding transitions.

single frequency—as a specific example, we choose a frequency of 2900 MHz. The angle η or the direction of the transverse component of the ac field can be determined by applying a static magnetic field of strength 10.7 mT in the plane perpendicular to the NV axis. The frequency of the transition $|0\rangle \longleftrightarrow |-\rangle$ at this field is 2900 MHz. The orientation of the static field at which this transition has the lowest intensity is the direction of the transverse component of the ac field. To determine the magnitude $B_{\rm ac}$ and the angle ζ, first we can measure the Rabi frequency of the transition $|0\rangle \longleftrightarrow |-\rangle$ in the static field of 10.7 mT oriented in the transverse plane with $\eta = \pi/2$. Next, a field of 146.1 mT can be applied in the transverse plane, with $\eta = 0$. This field mixes the states $|0\rangle$ and $|+\rangle$ and the new eigenstates are $|\alpha\rangle$, $|-\rangle$, and $|\beta\rangle$, where $|\alpha\rangle = 0.82|0\rangle - 0.58|+\rangle$ and $|\beta\rangle = 0.82|+\rangle + 0.58|0\rangle$. The state $|-\rangle$ does not mix with the other states, as it is an eigenstate of both the S_z^2 and S_x operators. The energy level diagram for this field orientation is given in Fig. 5. The frequency of the transition $|-\rangle \longleftrightarrow |\beta\rangle$ is 2900 MHz and it can be excited by the Y and Z components of the ac field. Since we already know the direction of the transverse component of the ac field, the Y component can be made equal to zero by orienting the static magnetic field along this direction. Note that the X axis is defined as the direction of the static field. So, for $\eta = 0$, the transition $|-\rangle \longleftrightarrow |\beta\rangle$ can only be excited by the Z component of the ac field. By measuring the Rabi frequency of this transition and using it in combination with the Rabi frequency of the transition $|0\rangle \longleftrightarrow |-\rangle$ at the field of 10.7 mT, we can determine the parameters $B_{\rm ac}$ and ζ. An important point to note here is that the mixing between the states $|0\rangle$ and $|+\rangle$ decreases the polarization of the electron spin under optical pumping and that in turn decreases the ODMR contrast.

In order to understand the change in spin contrast, we have measured the optical contrast of the Rabi oscillations when the static magnetic field is oriented perpendicular and parallel to the NV axis for different field strengths in the range 5–30 mT. The ratio of these contrasts (perpendicular/parallel) have been plotted in Fig. 6. As the field increases from 5 to 17 mT, the contrast of the transverse field orientation decreases by 2.5 times relative to the contrast of the parallel field orientation. Above 17 mT, the reduction in contrast continues at a slower
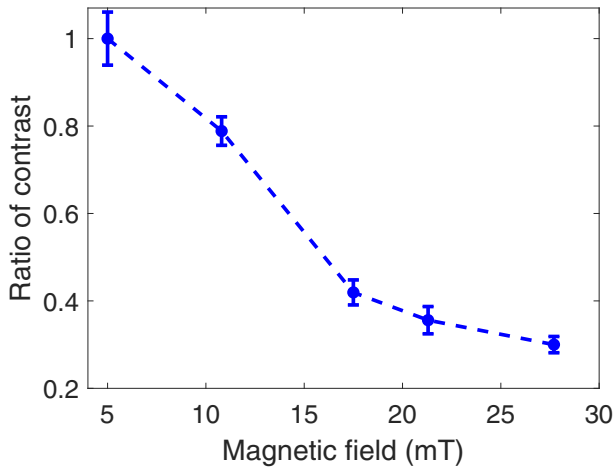
FIG. 6. Ratio of contrasts in the Rabi oscillations for the static magnetic field oriented perpendicular and parallel to the NV axis as a function of the field strength.

orientations of static field in the transverse plane, we can determine η, the azimuthal angle of the ac field. However, the amplitude of variation in these Rabi frequencies is proportional to the matrix element $|\langle -|S_y|\beta\rangle|$, which is very small for static fields of strength less than 10 mT. Hence, experimental determination of η for ac fields of frequency less than 30 MHz may be difficult.

In conclusion, we have proposed and experimentally demonstrated a method for the vector detection of ac fields by using NV centers having a single orientation. The method is equally applicable for single NV centers and is therefore more generally applicable than the conventional method using multiple NV centers with three different orientations. The static magnetic field control required in the current work is technically less demanding compared to the MW field control required in the rotating-frame Rabi method of Ref. [35]. The method is applicable over a wide frequency range, limited only by the achievable optical spin contrast at the transverse static field orientation. Since this method does not require NV centers of multiple orientations, it can be used for vector imaging of ac fields with nanoscale resolution. In particular, this method is suitable for vector ac field imaging by using single NV centers of diamond nanopillar probes attached to an atomic force microscope [12,49]. This work will also be useful for optimal control of quantum registers based on multiple dipolar coupled NV centers having different orientations in diamond. In such registers, it is not possible to align a static magnetic field with the NV axes of all the centers. Designing time-optimal quantum gates to the electron and ^{13}C nuclear spin qubits of misaligned NV centers requires accurate knowledge of the internal as well as the rf and MW control field Hamiltonians. The vector ac field detection scheme demonstrated in this work is useful for the precise determination of the control field Hamiltonian.

rate and it remains higher than in a similar case [48], where the angle between the NV axis and the magnetic field was kept at $\theta = 74°$.

The aforementioned procedure is intended for the vector detection of ac fields of frequency greater than 2870 MHz as this is the lowest frequency for the transitions $|0\rangle \longleftrightarrow |-\rangle$ and $|0\rangle \longleftrightarrow |+\rangle$. Now, we discuss the protocol for the vector detection of fields in the frequency range 1–2870 MHz. The frequency of the transition $|-\rangle \longleftrightarrow |\beta\rangle$ is in the frequency range 1–2870 MHz for static fields of strength 0–145 mT oriented perpendicular to the NV axis. This transition can be excited by only the Z component or by Z and Y components of the applied ac fields depending upon the strength and orientation of the static field in the transverse plane of the NV center. When a static field of strength 0–100 mT is applied parallel to the NV axis, the frequency of the transition $|0\rangle \longleftrightarrow |-1\rangle$ is in the range 1–2870 MHz and it can only be excited by the transverse components of the ac field. So, from the Rabi frequencies of the transitions $|-\rangle \longleftrightarrow |\beta\rangle$ and $|0\rangle \longleftrightarrow |-1\rangle$ at appropriate static magnetic fields, we can determine the strength of the ac field (B_{ac}) and the angle between the NV axis and the ac field (ζ). The Rabi frequency of the transition $|-\rangle \longleftrightarrow |\beta\rangle$ is proportional to $|\cos\zeta\langle -|S_z|\beta\rangle + \sin\zeta\sin\eta\langle -|S_y|\beta\rangle|$, which is minimum at $\eta = 0$ and maximum at $\eta = \pi/2$ for a fixed value of ζ. So, by measuring the Rabi frequency of this transition for different

[1] D. Budker and M. Romalis, Optical magnetometry, Nat. Phys. **3**, 227 (2007).

[2] M. Vengalattore, J. M. Higbie, S. R. Leslie, J. Guzman, L. E. Sadler, and D. M. Stamper-Kurn, High-resolution magnetometry with a spinor Bose-Einstein condensate, Phys. Rev. Lett. **98**, 200801 (2007).

[3] G. S. Waters and P. D. Francis, A nuclear magnetometer, J. Sci. Instrum. **35**, 88 (1958).

[4] R. L. Fagaly, Superconducting quantum interference device instruments and applications, Rev. Sci. Instrum. **77**, 101101 (2006).

[5] R. Schirhagl, K. Chang, M. Loretz, and C. L. Degen, Nitrogen-vacancy centers in diamond: Nanoscale sensors for physics and biology, Annu. Rev. Phys. Chem. **65**, 83 (2014).

[6] L. Rondin, J.-P. Tetienne, T. Hingant, J.-F. Roch, P. Maletinsky, and V. Jacques, Magnetometry with nitrogen-vacancy defects in diamond, Rep. Prog. Phys. **77**, 056503 (2014).

[7] S. Hong, M. S. Grinolds, L. M. Pham, D. L. Sage, L. Luan, R. L. Walsworth, and A. Yacoby, Nanoscale magnetometry with NV centers in diamond, MRS Bull. **38**, 155 (2013).

[8] G. Balasubramanian, I. Chan, R. Kolesov, M. Al-Hmoud, J. Tisler, C. Shin, C. Kim, A. Wojcik, P. R. Hemmer,

A. Krueger, T. Hanke, A. Leitenstorfer, R. Bratschitsch, F. Jelezko, and J. Wrachtrup, Nanoscale imaging magnetometry with diamond spins under ambient conditions, Nature (London) **455**, 648 (2008).

[9] C. L. Degen, Scanning magnetic field microscope with a diamond single-spin sensor, Appl. Phys. Lett. **92**, 243111 (2008).

[10] J. R. Maze, P. L. Stanwix, J. S. Hodges, S. Hong, J. M. Taylor, P. Cappellaro, L. Jiang, M. V. G. Dutt, E. Togan, A. S. Zibrov, A. Yacoby, R. L. Walsworth, and M. D. Lukin, Nanoscale magnetic sensing with an individual electronic spin in diamond, Nature (London) **455**, 644 (2008).

[11] T. Staudacher, F. Shi, S. Pezzagna, J. Meijer, J. Du, C. A. Meriles, F. Reinhard, and J. Wrachtrup, Nuclear magnetic resonance spectroscopy on a (5-nanometer)^3 sample volume, Science **339**, 561 (2013).

[12] P. Appel, M. Ganzhorn, E. Neu, and P. Maletinsky, Nanoscale microwave imaging with a single electron spin in diamond, New J. Phys. **17**, 112001 (2015).

[13] J. M. Boss, K. S. Cujia, J. Zopes, and C. L. Degen, Quantum sensing with arbitrary frequency resolution, Science **356**, 837 (2017).

[14] S. Schmitt, T. Gefen, F. M. Stürner, T. Unden, G. Wolff, C. Müller, J. Scheuer, B. Naydenov, M. Markham, S. Pezzagna, J. Meijer, I. Schwarz, M. Plenio, A. Retzker, L. P. McGuinness, and F. Jelezko, Submillihertz magnetic spectroscopy performed with a nanoscale quantum sensor, Science **356**, 832 (2017).

[15] J. Zhang and D. Suter, Single NV centers as sensors for radio-frequency fields, Phys. Rev. Res. **5**, L022026 (2023).

[16] R. C. Black, F. C. Wellstood, E. Dantsker, A. H. Miklich, D. Koelle, F. Ludwig, and J. Clarke, Imaging radio-frequency fields using a scanning SQUID microscope, Appl. Phys. Lett. **66**, 1267 (1995).

[17] V. Agrawal, P. Neuzil, and D. W. van der Weide, A microfabricated tip for simultaneous acquisition of sample topography and high-frequency magnetic field, Appl. Phys. Lett. **71**, 2343 (1997).

[18] S.-C. Lee, C. P. Vlahacos, B. J. Feenstra, A. Schwartz, D. E. Steinhauer, F. C. Wellstood, and S. M. Anlage, Magnetic permeability imaging of metals with a scanning near-field microwave microscope, Appl. Phys. Lett. **77**, 4404 (2000).

[19] P. Böhi, M. F. Riedel, T. W. Hänsch, and P. Treutlein, Imaging of microwave fields using ultracold atoms, Appl. Phys. Lett. **97**, 051101 (2010).

[20] P. Böhi and P. Treutlein, Simple microwave field imaging technique using hot atomic vapor cells, Appl. Phys. Lett. **101**, 181107 (2012).

[21] C. F. Ockeloen, R. Schmied, M. F. Riedel, and P. Treutlein, Quantum metrology with a scanning probe atom interferometer, Phys. Rev. Lett. **111**, 143001 (2013).

[22] T. van der Sar, F. Casola, R. Walsworth, and A. Yacoby, Nanometre-scale probing of spin waves using single electron spins, Nat. Commun. **6**, 7886 (2015).

[23] K. Chang, A. Eichler, J. Rhensius, L. Lorenzelli, and C. L. Degen, Nanoscale imaging of current density with a single-spin magnetometer, Nano Lett. **17**, 2367 (2017).

[24] F. Casola, T. van der Sar, and A. Yacoby, Probing condensed matter physics with magnetometry based on nitrogen-vacancy centres in diamond, Nat. Rev. Mater. **3**, 17088 (2018).

[25] B. J. Maertz, A. P. Wijnheijmer, G. D. Fuchs, M. E. Nowakowski, and D. D. Awschalom, Vector magnetic field microscopy using nitrogen vacancy centers in diamond, Appl. Phys. Lett. **96**, 092504 (2010).

[26] C. Zhang, H. Yuan, N. Zhang, L. Xu, J. Zhang, B. Li, and J. Fang, Vector magnetometer based on synchronous manipulation of nitrogen-vacancy centers in all crystal directions, J. Phys. D: Appl. Phys. **51**, 155102 (2018).

[27] H. Clevenson, L. M. Pham, C. Teale, K. Johnson, D. Englund, and D. Braje, Robust high-dynamic-range vector magnetometry with nitrogen-vacancy centers in diamond, Appl. Phys. Lett. **112**, 252406 (2018).

[28] J. M. Schloss, J. F. Barry, M. J. Turner, and R. L. Walsworth, Simultaneous broadband vector magnetometry using solid-state spins, Phys. Rev. Appl. **10**, 034044 (2018).

[29] H. Zheng, Z. Sun, G. Chatzidrosos, C. Zhang, K. Nakamura, H. Sumiya, T. Ohshima, J. Isoya, J. Wrachtrup, A. Wickenbrock, and D. Budker, Microwave-free vector magnetometry with nitrogen-vacancy centers along a single axis in diamond, Phys. Rev. Appl. **13**, 044023 (2020).

[30] D. A. Broadway, S. E. Lillie, S. C. Scholten, D. Rohner, N. Dontschuk, P. Maletinsky, J.-P. Tetienne, and L. C. L. Hollenberg, Improved current density and magnetization reconstruction through vector magnetic field measurements, Phys. Rev. Appl. **14**, 024076 (2020).

[31] T. Weggler, C. Ganslmayer, F. Frank, T. Eilert, F. Jelezko, and J. Michaelis, Determination of the three-dimensional magnetic field vector orientation with nitrogen vacancy centers in diamond, Nano Lett. **20**, 2980 (2020).

[32] B. Chen, X. Hou, F. Ge, X. Zhang, Y. Ji, H. Li, P. Qian, Y. Wang, N. Xu, and J. Du, Calibration-free vector magnetometry using nitrogen-vacancy center in diamond integrated with optical vortex beam, Nano Lett. **20**, 8267 (2020).

[33] P. Reuschel, M. Agio, and A. M. Flatae, Vector magnetometry based on polarimetric optically detected magnetic resonance, Adv. Quantum Technol. **5**, 2200077 (2022).

[34] P. Wang, Z. Yuan, P. Huang, X. Rong, M. Wang, X. Xu, C. Duan, C. Ju, F. Shi, and J. Du, High-resolution vector microwave magnetometry based on solid-state spins in diamond, Nat. Commun. **6**, 6631 (2015).

[35] G. Wang, Y.-X. Liu, Y. Zhu, and P. Cappellaro, Nanoscale vector ac magnetometry with a single nitrogen-vacancy center in diamond, Nano Lett. **21**, 5143 (2021).

[36] K. R. K. Rao and D. Suter, Level anti-crossings of a nitrogen-vacancy center in diamond: decoherence-free subspaces and 3D sensors of microwave magnetic fields, New J. Phys. **22**, 103065 (2020).

[37] F. Dolde, H. Fedder, M. W. Doherty, T. Nobauer, F. Rempp, G. Balasubramanian, T. Wolf, F. Reinhard, L. C. L. Hollenberg, F. Jelezko, and J. Wrachtrup, Electric-field sensing using single diamond spins, Nat. Phys. **7**, 459 (2011).

[38] C. S. Shin, C. E. Avalos, M. C. Butler, H.-J. Wang, S. J. Seltzer, R.-B. Liu, A. Pines, and V. S. Bajaj, Suppression of electron spin decoherence of the diamond NV center by a transverse magnetic field, Phys. Rev. B **88**, 161412(R) (2013).

[39] E. Moreva, E. Bernardi, P. Traina, A. Sosso, S. D. Tchernij, J. Forneris, F. Picollo, G. Brida, i. c. v. Pastuović, I. P. Degiovanni, P. Olivero, and M. Genovese, Practical applications of quantum sensing: A simple method to enhance the sensitivity of

nitrogen-vacancy-based temperature sensors, Phys. Rev. Appl. **13**, 054057 (2020).

[40] Z. Qiu, U. Vool, A. Hamo, and A. Yacoby, Nuclear spin assisted magnetic field angle sensing, npj Quantum Inf. **7**, 39 (2021).

[41] M. W. Doherty, N. B. Manson, P. Delaney, F. Jelezko, J. Wrachtrup, and L. C. Hollenberg, The nitrogen-vacancy colour centre in diamond, Phys. Rep. **528**, 1 (2013).

[42] D. Suter and F. Jelezko, Single-spin magnetic resonance in the nitrogen-vacancy center of diamond, Prog. Nucl. Magn. Reson. Spectrosc. **98-99**, 50 (2017).

[43] F. Bitter, The optical detection of radiofrequency resonance, Phys. Rev. **76**, 833 (1949).

[44] D. Suter, Optical detection of magnetic resonance, Magn. Reson. **1**, 115 (2020).

[45] J. M. Taylor, P. Cappellaro, L. Childress, L. Jiang, D. Budker, P. R. Hemmer, A. Yacoby, R. Walsworth, and M. D. Lukin, High-sensitivity diamond magnetometer with nanoscale resolution, Nat. Phys. **4**, 810 (2008).

[46] R. S. Schoenfeld and W. Harneit, Real time magnetic field sensing and imaging using a single spin in diamond, Phys. Rev. Lett. **106**, 030802 (2011).

[47] A. Dréau, M. Lesik, L. Rondin, P. Spinicelli, O. Arcizet, J.-F. Roch, and V. Jacques, Avoiding power broadening in optically detected magnetic resonance of single NV defects for enhanced dc magnetic field sensitivity, Phys. Rev. B **84**, 195204 (2011).

[48] J.-P. Tetienne, L. Rondin, P. Spinicelli, M. Chipaux, T. Debuisschert, J.-F. Roch, and V. Jacques, Magnetic-field-dependent photodynamics of single NV defects in diamond: an application to qualitative all-optical magnetic imaging, New J. Phys. **14**, 103033 (2012).

[49] P. Maletinsky, S. Hong, M. S. Grinolds, B. Hausmann, M. D. Lukin, R. L. Walsworth, M. Loncar, and A. Yacoby, A robust scanning diamond sensor for nanoscale imaging with single nitrogen-vacancy centres, Nat. Nanotechnol. **7**, 320 (2012).